SCIENTIFIC REPORTS

OPEN

Fluorescence via Reverse Intersystem Crossing from Higher Triplet States in a Bisanthracene Derivative

Received: 23 December 2016
Accepted: 23 May 2017
Published online: 06 July 2017

Tohru Sato[1,2], Rika Hayashi[3], Naoki Haruta[1] & Yong-Jin Pu[4,5]

To elucidate the high external quantum efficiency observed for organic light-emitting diodes using a bisanthracene derivative (BD1), non-radiative transition processes as well as radiative ones are discussed employing time-dependent density functional theory. It has been previously reported that the observed high external quantum efficiency of BD1 cannot be explained by the conventional thermally activated delayed fluorescence involving T_1 exciton nor triplet-triplet annihilation. The calculated off-diagonal vibronic coupling constants of BD1, which govern the non-radiative transition rates, suggest *a fluorescence via higher triplets* (*FvHT*) *mechanism*, which entails the conversion of a high triplet exciton generated during electrical excitation into a fluorescent singlet exciton. This mechanism is valid as long as the relaxation of high triplet states to lower states is suppressed. In the case of BD1, its pseudo-degenerate electronic structure helps the suppression. A general condition is also discussed for the suppression of transitions in molecules with pseudo-degenerate electronic structures.

Thermally activated delayed fluorescence (TADF) has attracted significant attention as the emission mechanism in molecules used in organic light-emitting diodes (OLEDs)[1]. Although the phenomenon of TADF has been known for a long time, its application in OLEDs was first reported by Endo *et al.* in 2009[2]. TADF OLEDs utilize fluorescence via reverse intersystem crossing (RISC) from the triplet state, T_1, generated during electrical excitation, as well as fluorescence from the singlet excited state, S_1, generated during electrical excitation.

In order to make RISC possible in a molecule, the energy difference between S_1 and T_1, ΔE_{ST}, must be small enough that the RISC energy barrier can be overcome through thermal excitation. ΔE_{ST} can be written as

$$\Delta E_{ST} = 2J = 2 \iint \psi^*_{HO}(r_1)\psi_{LU}(r_1)\frac{1}{r_{12}}\psi_{HO}(r_2)\psi^*_{LU}(r_2)d^3r_1 d^3r_2, \quad (1)$$

where J is an exchange integral, and $\psi_{HO}(r)$ and $\psi_{LU}(r)$ denote the HOMO and LUMO, respectively. Based on this equation, Endo *et al.* proposed a design principle to reduce ΔE_{ST}[2], i.e. candidates for TADF molecules must be donor-acceptor systems with small overlap between the HOMO and LUMO.

Based on this design principle for emitting molecules, a number of TADF OLEDs have exhibited very high external quantum efficiencies (EQEs). For example, a phenoxazine derivative, PXZ-TRZ, exhibits an EQE of 12.5% (photoluminescence quantum efficiency (PLQE): 65.7%)[3], a carbazolyl dicyanobenzene derivative, 4CzIPN, exhibits an EQE of 19.3% (PLQE: 94%)[4], a triazine derivative, CC2TA, exhibits an EQE of 11% (PLQE: 62%)[5], a spiro bifluorene derivative, Spiro-CN, exhibits an EQE of 4.4% (PLQE: 27%)[6], and an acridine derivative, ACRFLCN, exhibits an EQE of 10.1% (PLQE: 67%)[7]. Recently, Kaji *et al.* reported a triazine derivative, DACT-II, exhibiting an extremely high EQE of 41.5% (PLQE:100%)[8]. These results demonstrate the success of this design principle.

[1]Department of Molecular Engineering, Graduate School of Engineering, Kyoto University, Nishikyo-ku, Kyoto, 615-8510, Japan. [2]Unit of Elements Strategy Initiative for Catalysts & Batteries, Kyoto University, Nishikyo-ku, Kyoto, 615-8510, Japan. [3]Undergraduate School of Industrial Chemistry, Faculty of Engineering, Kyoto University, Sakyo-ku, Kyoto, 606-8501, Japan. [4]Graduate School of Organic Materials Science, Yamagata University, Yonezawa, 992-8510, Yamagata, Japan. [5]PRESTO (Sakigake), JST, Kawaguchi, Saitama, 332-0012, Japan. Correspondence and requests for materials should be addressed to T.S. (email: tsato@moleng.kyoto-u.ac.jp)

However, this design principle also has certain drawbacks: (1) the small overlap between the HOMO and LUMO leads to suppression of the oscillator strength[9,10], and (2) TADF OLEDs exhibit broad emission wavelengths because of charge-transfer (CT) excitation. In order to overcome these drawbacks, Sato *et al.* proposed other concepts for emitting molecules in OLEDs, viz. symmetry-controlled TADF (SC-TADF) and inverted singlet and triplet (iST) structure, wherein fluorescence via RISC from triplet states higher than T_1 is utilized based on the selection rules of transition dipole moment (TDM) and spin-orbit coupling (SOC)[11]. The order of the preferable point groups for realizing SC-TADF and iST is as follows:

$$\begin{aligned} D_{6h} > O_h > I_h = D_{4h} > D_{2h} > D_{3h} > T_d > C_i = C_{2h} > D_{2d} = C_{4v} > D_2 \\ = C_{2v} > C_{3v} > C_s = C_1. \end{aligned} \tag{2}$$

These mechanisms are unlike TADF because they enable us to (1) use candidates not belonging to the donor-acceptor type and (2) induce RISC without thermal excitation. Uejima *et al.* and Sato *et al.* have already designed and proposed iST molecules based on anthracene[9,10] and perylene derivatives[11], respectively.

The concepts of SC-TADF and iST require a high molecular symmetry group. However, even for asymmetric molecules, RISC via higher T_n is possible as long as undesirable interactions are suppressed. Recently, a phenothiazin-benzothiadiazole derivative, PTZ-BZP, used as a fluorescent OLED exhibited a high EQE of 1.54% (PLQE:16%)[12], which was attributed to fluorescence via RISC from T_3 based on the energy gap law. Sato also proposed that the high EQE in PTZ-BZP, which is an asymmetric molecule, can be attributed to suppressed radiative and non-radiative transitions from triplet states higher than T_1 to lower triplet states because of small overlap densities in the pseudo-degenerate electronic structure as well as the small energy gap between the relevant triplet and singlet states[13].

The overlap density ρ^{mn} between the N-electron wave functions of electronic states Ψ_m and Ψ_n is defined by

$$\rho^{mn}(r_i) := N \int \cdots \int \Psi_m^*(R_0, r)\Psi_n(R_0, r) d^4x_1 \cdots d^4x_{i-1} ds_i d^4x_{i+1} \cdots d^4x_N, \tag{3}$$

where R_0 denotes a reference nuclear configuration, and $x_i = (r_i, s_i)$ with spatial coordinate r_i and spin coordinate s_i for electron i[9,10]. Hereafter r_i is simply denoted as r. $\rho^{mn}(r)$ is sometimes called a transition density[14], especially within the orbital approximation. For example, in the case of the HOMO-LUMO transition, it is equal to HOMO-LUMO overlap density. The overlap density is related to the rate constants of radiative and non-radiative transitions as follows.

The rate constant of the radiative transition between electronic states m and n depends on the square of TDM, μ_{mn}, defined as

$$\mu_{mn} := \int \cdots \int \Psi_m^*(R_0, r) \left(\sum_i -er_i \right) \Psi_n(R_0, r) d^4x_1 \cdots d^4x_N, \tag{4}$$

while that of the non-radiative transition via vibrational mode α depends on the square of off-diagonal vibronic coupling constant (VCC) V_α^{mn}, defined as

$$V_\alpha^{mn} := \int \cdots \int \Psi_m^*(R_0, r) \left(\frac{\partial \hat{H}}{\partial Q_\alpha} \right)_{R_0} \Psi_n(R_0, r) d^4x_1 \cdots d^4x_N, \tag{5}$$

where e denotes the elementary charge, $\hat{H}$ is a molecular Hamiltonian, and Q_α stands for a mass-weighted normal coordinate of mode α[9,10]. TDM μ_{mn} and off-diagonal VCC V_α^{mn} represent the strengths of radiative and non-radiative transitions, respectively. The relations of the transition rate constants to μ_{mn} and V_α^{mn} are described in more detail in Section S1 of the Supplemental Material. These rate constants were also derived on the basis of the Born–Oppenheimer approximation in past literatures[15,16]. It should be noted that the present expression of the non-radiative rate constant is different from the other authors'[15,16]. Eq. (5) is based on the crude adiabatic approximation[17].

TDM μ_{mn} can be rewritten using the transition dipole moment density (TDMD) $\tau_{mn}(r)$:

$$\mu_{mn} = \int \tau_{mn}(r) d^3r, \tag{6}$$

where the TDMD is defined by

$$\tau_{mn}(r) := -er\rho^{mn}(r). \tag{7}$$

TDMD $\tau_{mn}(r)$ illustrates the origin of TDM which causes radiative transition as a local picture. The detailed derivation of TDMD is shown in Section S2 of the Supplemental Material. The off-diagonal VCC V_α^{mn} can be exactly expressed using the off-diagonal vibronic coupling density (VCD) $\eta_\alpha^{mn}(r)$[9,10]:

$$V_\alpha^{mn} = \int \eta_\alpha^{mn}(r) d^3r, \tag{8}$$

where the off-diagonal VCD is defined by

$$\eta_\alpha^{mn}(r) := \rho^{mn}(r) \times v_\alpha(r), \tag{9}$$

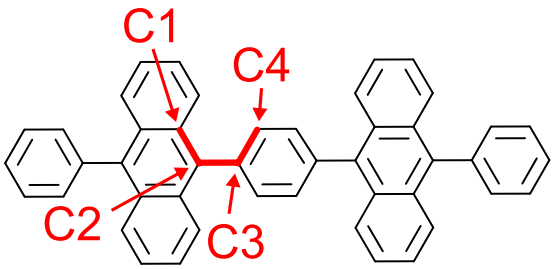

Figure 1. Bisanthracene derivative, BD1.

and the potential derivative $v_\alpha(r)$ is defined by

$$v_\alpha(r) := \left(\frac{\partial u(r)}{\partial Q_\alpha}\right)_{R_0}, \quad u(r) := \sum_{A=1}^{M} -\frac{Z_A e^2}{4\pi\varepsilon_0 |r - R_A|}, \tag{10}$$

where $u(r)$ is the attractive potential of a single electron due to all nuclei, and R_A and Z_A are the position and charge of nucleus A. VCD $\eta_\alpha^{mn}(r)$ illustrates the origin of VCC which gives rise to non-radiative transition as a local picture. The detailed derivation of VCD can be found in Section S2 of the Supplemental Material. Based on Eqs (6), (7), (8) and (9), both radiative and non-radiative transitions are suppressed when the overlap density $\rho^{mn}(r)$ is small. As mentioned earlier, the unusual high EQE in PTZ-BZP[12] has been successfully explained using the concept of the overlap density[13].

Recently, Hu *et al*. have observed blue-light emission in OLEDs using bisanthracene derivatives including 1,4-bis(10-phenylanthracene-9-yl)benzene (BD1) (see Fig. 1)[18]. Since the observed PLQE of BD1 is 14% in the neat film while the maximum EQE is 8.9% in the doped film, the emission is not conventional fluorescence using only singlet excitons. In other words, triplet excitons must contribute to the observed emission. However, the detailed mechanism of the observed high EQE is still unclear. Although one possible mechanism is the TADF, ΔE_{ST} between S_1 and T_1 was calculated to be too large to be overcome thermally[18]. Therefore, the conventional TADF involving T_1 is invalid. Another possible mechanism is the triplet-triplet annihilation (TTA). In the TTA mechanism, 62.5% of generated excitons can be used as fluorescent singlet excitons at best. Hu *et al*. have reported that the observed PLQE of the neat film is 14%[18]. Using these values, the estimated upper-limit of the EQE is 1.8–3.5% even if the outcoupling efficiency is assumed to be 20–40%. However, the highest EQE value was reported to be 5.6% in the device employing a neat film of BD1 as an emitting layer. Therefore, we cannot explain the observed EQE on the basis of the TTA mechanism. The other mechanism is required to explain the observed EQE of BD1.

In this study, we theoretically investigate the mechanism of light emission from an OLED using a bisanthracene derivative, BD1, on the basis of the understanding of radiative and non-radiative transition processes. We propose *a fluorescence via higher triplets* (*FvHT*) mechanism to explain the high EQE in OLEDs using BD1. FvHT is valid as long as undesirable radiative and non-radiative transitions are suppressed. In this mechanism, the concept of overlap density plays a crucial role. In addition, we perform the analyses for electronic wave functions of BD1 in detail to obtain general design principles for the realization of the present mechanism.

Results

The symmetry of the optimized structure for the ground state is not D_{2h} but D_2 because the dihedral angle (C1–C2–C3–C4) between the anthracene and benzene moieties (see Fig. 1) is not the right angle, as shown in Figs. S1 and S2 in the Supplemental Material. Therefore, it is not suitable as an iST nor SC-TADF molecule, as expressed in Eq. (2) (see also Section S4 of the Supplemental Material).

Frontier orbitals and their energy levels at the optimized structure of the ground state are shown in Fig. 2. The NHOMO ψ_{NHO} and HOMO ψ_{HO} as well as the NLUMO ψ_{NLU} and LUMO ψ_{LU} are pseudo-degenerate, respectively. This is because these orbitals consist of the fragment orbitals localized on the anthracene moieties. From Fig. 2, the frontier orbitals can be approximately represented as follows:

$$\psi_{LU} \approx \frac{1}{\sqrt{2}}(\phi_{LU}(L) - \phi_{LU}(R)), \qquad \psi_{NLU} \approx \frac{1}{\sqrt{2}}(\phi_{LU}(L) + \phi_{LU}(R)), \tag{11}$$

$$\psi_{HO} \approx \frac{1}{\sqrt{2}}(\phi_{HO}(L) + \phi_{HO}(R)), \qquad \psi_{NHO} \approx \frac{1}{\sqrt{2}}(\phi_{HO}(L) - \phi_{HO}(R)), \tag{12}$$

where $\phi_{HO/LU}(L/R)$ denotes the fragment MOs consisting of the HOMO/LUMO of the anthracene moiety Left(L)/Right(R). These approximate expressions of the frontier orbitals will be used later.

Franck–Condon (FC) excited states were calculated at the optimized structure for S_0. Figure 3 shows the energy levels of the FC states. The singlet and triplet excited states from S_1 to S_4 and from T_1 to T_4 mainly consist of linear combinations of one-electron excited configurations of HOMO → LUMO, HOMO → NLUMO, NHOMO → LUMO, and NHOMO → NLUMO. The energy levels of T_3 and T_4 are close to those of S_1, S_2, S_3, and S_4.

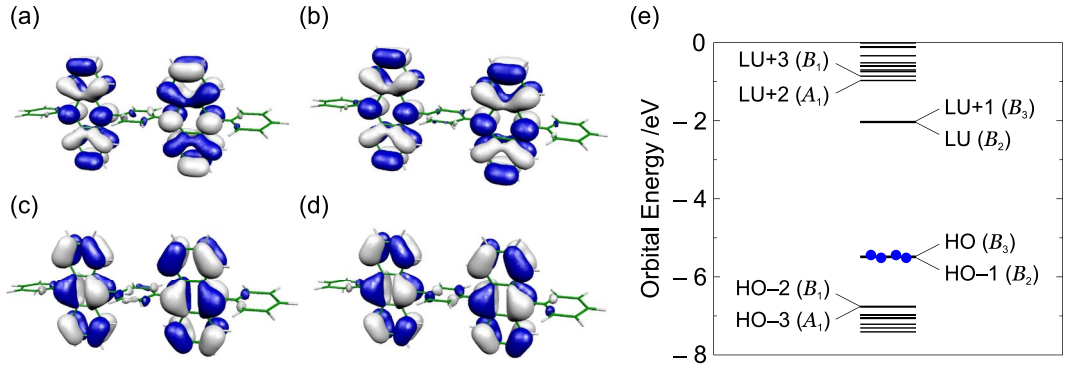

Figure 2. Frontier orbitals of BD1: (**a**) B_2 LUMO, (**b**) B_3 NLUMO, (**c**) B_3 HOMO, and (**d**) B_2 NHOMO. The isosurface value is 2.0×10^{-2} a.u. (**e**) Frontier orbital levels of BD1. It should be noted that the HOMO and next HOMO as well as the LUMO and next LUMO are pseudo-degenerate, respectively.

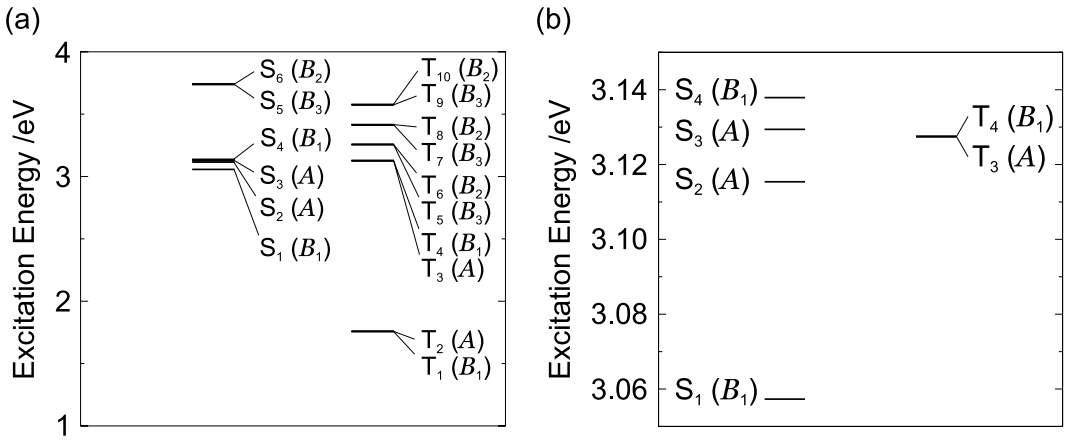

Figure 3. (**a**) Energy levels of the excited states in BD1 at the optimized structure for S_0, and (**b**) an enlarged view of the relevant levels.

On the other hand, the energy levels of T_1 and T_2 are much lower than that of the lowest singlet excited state. Therefore, the TADF from the T_1 and T_2 states is not possible, as reported previously[18].

In order to investigate roles of the higher excited states, the geometrical structures of T_4, T_3, S_4, S_3, S_2, and S_1 were optimized to discuss radiative and non-radiative transitions from the adiabatic excited states. Figures S1 and S2 in the Supplemental Material show the optimized structures of the relevant excited states. All the optimized structures show D_2 symmetry. The T_4 state has lower energy than T_3 at the T_n optimized structure ($n = 3, 4$), as shown in Fig. S3 in Section S5 of the Supplemental Material. Hereafter, we will refer to the electronic state at a certain geometry corresponding to the T_n FC state as T_n.

Figures 4(a) and (b) show the energy levels of the excited states at the optimized structures for T_3 and T_4. Table 1 lists the triplet excited states at the optimized structure for T_3. The selection rules are summarized in Section S6 of the Supplemental Material. Although T_3 is close to S_2 with $\Delta E_{T_3-S_2} = 0.8$ meV, RISC between T_3 and S_2 is symmetry forbidden (see Table S5). The electric dipole transition $T_3 \rightarrow T_4$ and internal conversion (IC) $T_3 \rightarrow T_4$ via b_1 modes are allowed. Therefore, if the transition probability of $T_3 \rightarrow T_4$ is large, a T_3 exciton generated during electrical excitation is immediately converted into a T_4 exciton. The transition rate will be discussed later by calculating off-diagonal VCCs.

Table S7 of the Supplemental Material lists the triplet excited states at the optimized structure for T_4. T_4 is close to S_2 with $\Delta E_{S_2-T_4} = 21$ meV, and RISC between T_4 and S_2 is symmetry allowed. Although the electric dipole transition $T_4 \rightarrow T_1$ is symmetry forbidden, that between T_4 and T_2 is symmetry allowed. In addition, IC $T_4 \rightarrow T_2$ with the help of b_1 modes and IC $T_4 \rightarrow T_1$ with the help of α modes are symmetry allowed. Only if the transitions of $T_4 \rightarrow T_2$ and $T_4 \rightarrow T_1$ are suppressed, a T_4 exciton can be up-converted into an S_2 exciton with thermal excitation. Otherwise, a T_4 exciton is immediately relaxed into a T_1 or T_2 exciton, resulting in the decrease of the EQE. The validity of this up-conversion path will be confirmed later by calculating off-diagonal VCCs.

The exciton dynamics is also important after the up-conversion of a T_4 exciton into a S_2 exciton. Figure 4(c) and (d) show the energy levels of the excited states at the optimized structures for S_2 and S_1. The singlet states at the optimized structure for S_2 are tabulated in Table S8 of the Supplemental Material. IC $S_2 \rightarrow S_0$ via a modes and IC $S_2 \rightarrow S_1$ via b_1 modes are symmetry allowed. The electric dipole transition $S_2 \rightarrow S_0$ is symmetry forbidden. On

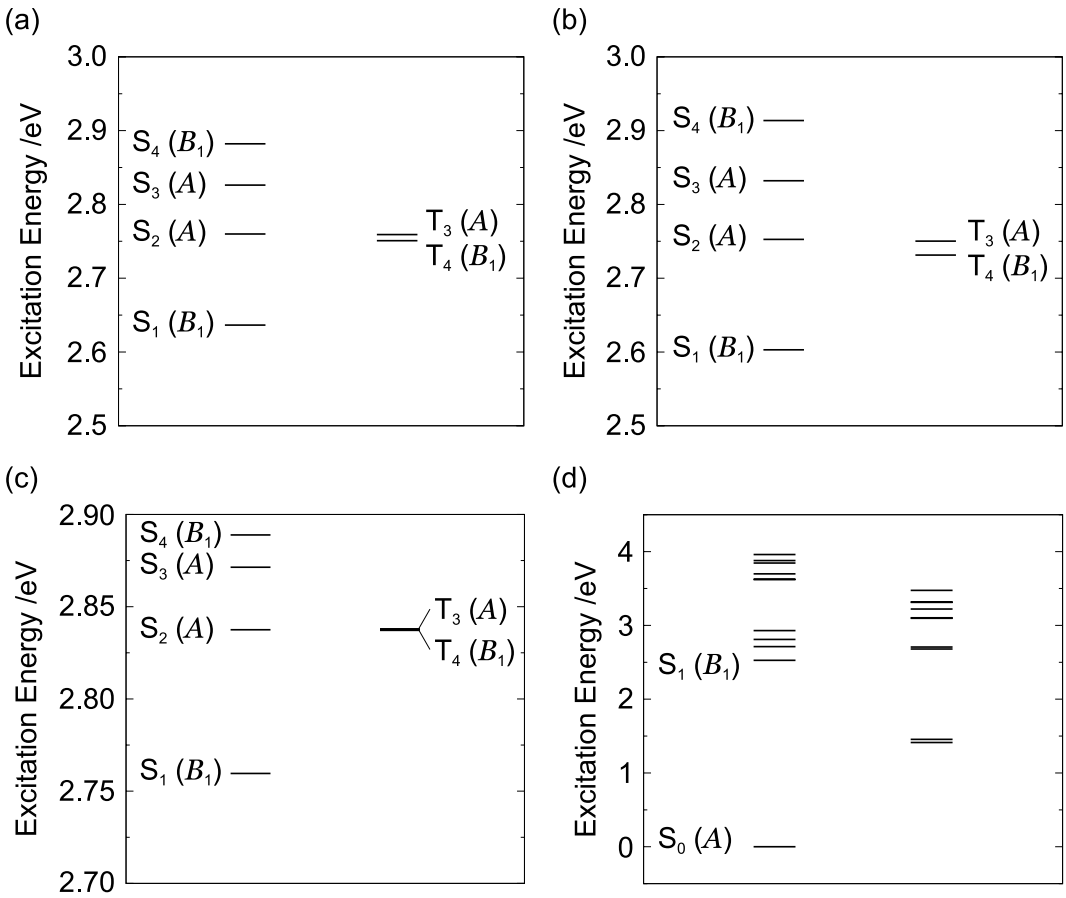

Figure 4. Energy levels of excited states at the optimized structures for (**a**) T_3, (**b**) T_4, (**c**) S_2, and (**d**) S_1.

	Excitation Energy		Major Configuration (CI Coefficient)
	eV	nm	
$T_4(B_1)$	2.7508	450.72	HO−1 → LU + 1(0.524),HO → LU(−0.455)
$T_3(A)$	2.7591	449.37	HO−1 → LU(−0.501),HO → LU + 1(0.496)
$T_2(A)$	1.4403	860.84	HO → LU + 1(0.502),HO−1 → LU(0.497)
$T_1(B_1)$	1.4252	869.93	HO → LU(−0.539),HO−1 → LU + 1(−0.458)

Table 1. Triplet excited states at the optimized structure for T_3.

the other hand, the electric dipole transition $S_2 \rightarrow S_1$ is symmetry allowed. Therefore, if the transition probability of IC $S_2 \rightarrow S_0$ is small, an S_2 exciton is relaxed into the S_1 state. The singlet states at the optimized structure for S_1 are listed in Table S9 of the Supplemental Material. S_1 belongs to the B_1 irreducible representation and is the fluorescent state, as indicated by the oscillator strengths f listed in Table S9 of the Supplemental Material.

As discussed above, if the transition probability of $T_3 \rightarrow T_4$ is large, those of $T_4 \rightarrow T_2$ and $T_4 \rightarrow T_1$ are small, and that of $S_2 \rightarrow S_0$ is small, then, the FvHT mechanism is possible: the high triplet excitons, T_3 and T_4, can be effectively converted into a fluorescent S_1 exciton. The calculated off-diagonal VCCs are shown in Fig. 5. Vibrational modes with strong couplings are shown in Section S8 of the Supplemental Material. From Fig. 5, the transition probabilities of the ICs are in the following order:

$$T_3 \rightarrow T_4 > S_2 \rightarrow S_1 \gg S_1 \rightarrow S_0 \gg S_2 \rightarrow S_0 > T_4 \rightarrow T_1 > T_4 \rightarrow T_2. \quad (13)$$

Based on the discussion of the adiabatic excited states and Eq. (13), the scheme of excited state dynamics is depicted in Fig. 6. From Fig. 5 and Eq. (13), the transition probabilities of these undesirable non-radiative processes for the present FvHT mechanism, $S_2 \rightarrow S_0$, $T_4 \rightarrow T_1$, and $T_4 \rightarrow T_2$, are small. This is due to the disappearance of the overlap densities, as discussed later. It should be noted that the transition probabilities of the radiative transitions of $S_2 \rightarrow S_0$, $T_4 \rightarrow T_1$, and $T_4 \rightarrow T_2$ are also small, because the TDMs as well as the VCCs depend on the overlap densities. On the other hand, the non-radiative transition probabilities of the ICs $S_2 \rightarrow S_1$ and $T_3 \rightarrow T_4$ are large. In addition, the transition probability of IC $S_1 \rightarrow S_0$ is small enough for a S_1 exciton to emit fluorescence.

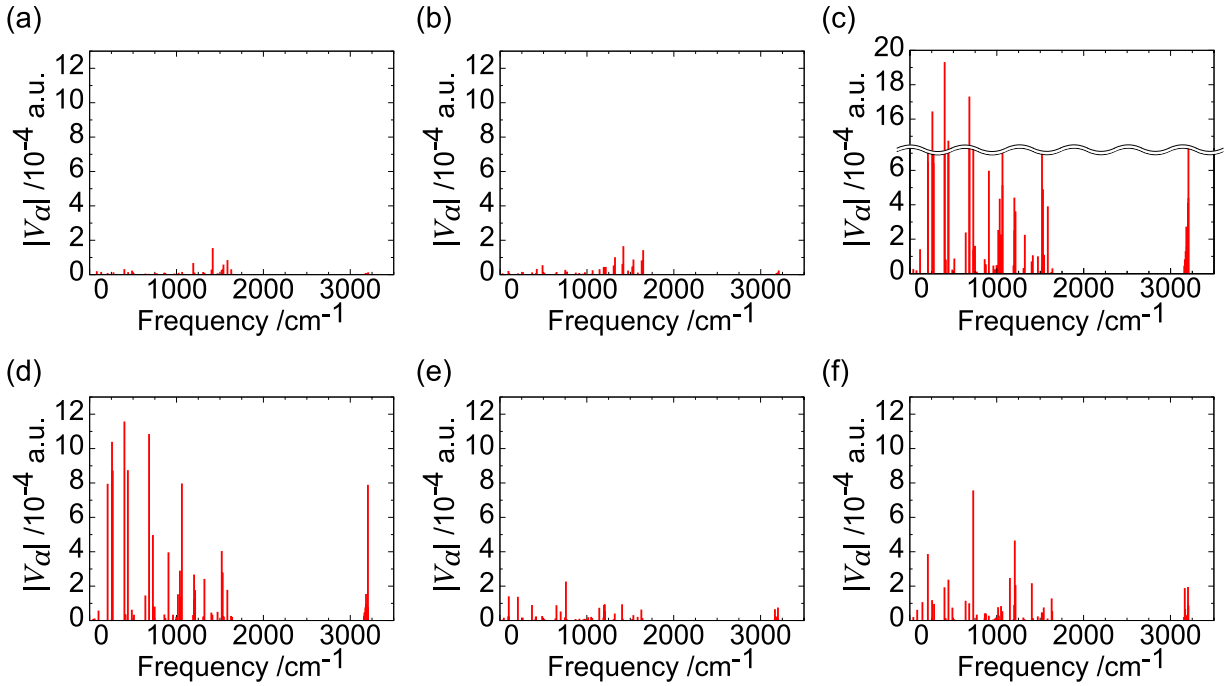

Figure 5. Off-diagonal VCCs of (**a**) $T_4@T_4 \rightarrow T_2@T_4$, (**b**) $T_4@T_4 \rightarrow T_1@T_4$, (**c**) $T_3@T_3 \rightarrow T_4@T_3$, (**d**) $S_2@S_2 \rightarrow S_1@S_2$, (**e**) $S_2@S_2 \rightarrow S_0@S_2$, and (**f**) $S_1@S_1 \rightarrow S_0@S_1$. $@T_n/@S_n$ denote the geometry used in optimization for the T_n/S_n state.

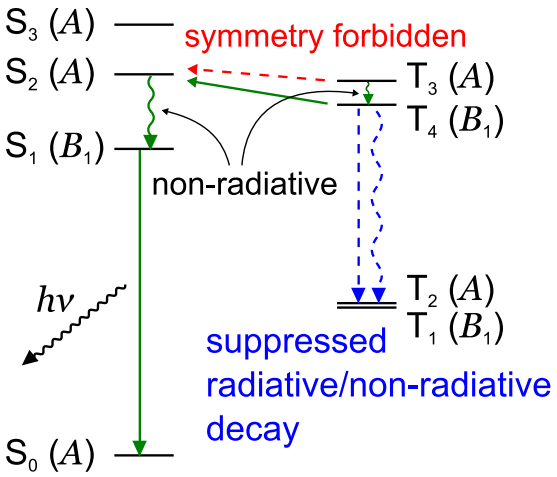

Figure 6. Scheme of the excited state dynamics in BD1. Horizontal solid arrows indicate RISC, vertical straight arrows indicate radiative transitions, and wavy arrows denote non-radiative transitions.

Accordingly, we can conclude that both T_3 and T_4 excitons generated during electrical excitation are effectively converted into a fluorescent S_1 exciton.

Discussion

As was discussed in the previous section, the off-diagonal VCCs for T_3–T_4 and S_2–S_1 are large. On the other hand, the off-diagonal VCCs for T_4–T_2, T_4–T_1, and S_2–S_0 are small. These VCCs are the origin of the present FvHT mechanism. Figure 7 shows the overlap densities having the same isosurface values. Among them, the overlap densities for T_4–T_2, T_4–T_1, and S_2–S_0 disappear. This is the reason why the transitions of $T_4 \rightarrow T_2$, $T_4 \rightarrow T_1$, and $S_2 \rightarrow S_0$ are suppressed (see also vibronic coupling density analyses for these transitions in Section S9 of the Supplemental Material). In this section, we discuss the disappearance mechanism of these overlap densities.

A TD-DFT wave function is given by

$$\Psi_n = \sum_{i \in \mathrm{occ}} \sum_{r \in \mathrm{unocc}} C_i^r \Phi_i^r, \tag{14}$$

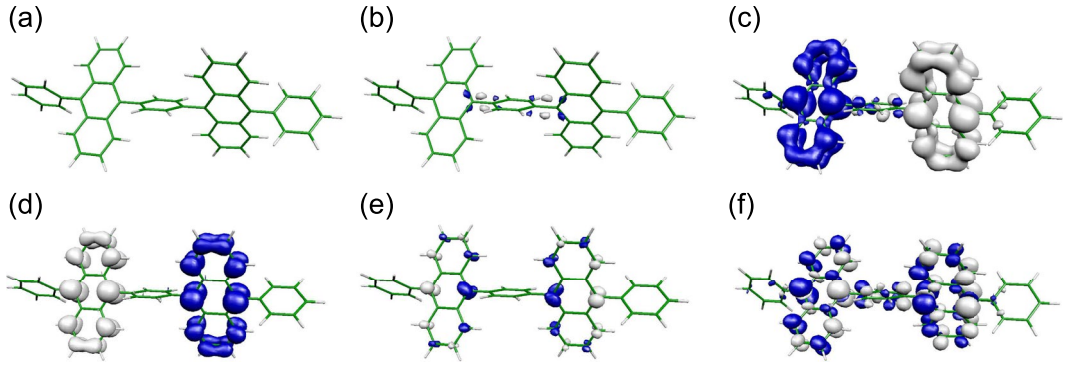

Figure 7. Overlap densities for (**a**) $T_4@T_4$–$T_2@T_4$, (**b**) $T_4@T_4$–$T_1@T_4$, (**c**) $T_3@T_3$–$T_4@T_3$, (**d**) $S_2@S_2$–$S_1@S_2$, (**e**) $S_2@S_2$–$S_0@S_2$, and (**f**) $S_1@S_1$–$S_0@S_1$, respectively. All isosurface values are the same, i.e. 1.0×10^{-3} a.u.

where Φ_i^r represents the electronic configuration of a single-electron excitation from occupied orbital i to vacant orbital r, and C_i^r represents the CI coefficient. The overlap density between two excited states Ψ_m and Ψ_n, ρ^{mn}, is given by

$$\rho^{mn} = \sum_{i\in \mathrm{occ}} \sum_{r\in \mathrm{unocc}} \sum_{j\in \mathrm{occ}} \sum_{s\in \mathrm{unocc}} D_j^{s*} C_i^r \rho\left(\Phi_j^s, \Phi_i^r\right), \tag{15}$$

where D_j^s is the CI coefficient of another excited state m, and $\rho(\Phi_j^s, \Phi_i^r)$ denotes the overlap density between the two configurations.

Φ_0 represents a ground state electron configuration, and its overlap density ρ_0 is given by

$$\rho(\Phi_0, \Phi_0) =: \rho_0. \tag{16}$$

The overlap densities for various configurations are summarized as follows,

$$\rho(\Phi_i^r, \Phi_i^r) = \rho_0 - |\psi_i|^2 + |\psi_r|^2, \quad \rho(\Phi_0, \Phi_i^r) = \psi_i^* \psi_r, \quad \rho(\Phi_i^r, \Phi_j^r) = \psi_i^* \psi_j \quad (i \neq j), \tag{17}$$

$$\rho(\Phi_i^r, \Phi_i^s) = \psi_r^* \psi_s \quad (r \neq s), \quad \rho(\Phi_i^r, \Phi_j^s) = 0 \quad (i \neq j, r \neq s), \tag{18}$$

where ψ represents a molecular orbital.

According to Tables 1, S7, S8, and S9, the approximate wave functions for the relevant excited states can be written as follows:

$$\Psi_a = C_1^a \Phi_{\mathrm{HO}}^{\mathrm{LU}} + C_2^a \Phi_{\mathrm{NHO}}^{\mathrm{NLU}}, \quad (\mathrm{T}_4) \tag{19}$$

$$\Psi_b = C_3^b \Phi_{\mathrm{HO}}^{\mathrm{NLU}} + C_4^b \Phi_{\mathrm{NHO}}^{\mathrm{LU}}, \quad (\mathrm{S}_2) \tag{20}$$

$$\Psi_c = C_1^c \Phi_{\mathrm{HO}}^{\mathrm{LU}} + C_2^c \Phi_{\mathrm{NHO}}^{\mathrm{NLU}}, \quad (\mathrm{T}_1) \tag{21}$$

$$\Psi_d = \Phi_{\mathrm{HO}}^{\mathrm{LU}}, \quad (\mathrm{S}_1) \tag{22}$$

$$\Psi_e = C_3^e \Phi_{\mathrm{HO}}^{\mathrm{NLU}} + C_4^e \Phi_{\mathrm{NHO}}^{\mathrm{LU}}, \quad (\mathrm{T}_2) \tag{23}$$

$$\Psi_0 = \Phi_0, \quad (\mathrm{S}_0) \tag{24}$$

where the set of the CI coefficients is assumed to satisfy the following relation:

$$C_1^a \approx -C_2^a \approx C_3^b \approx -C_4^b \approx C_1^c \approx C_2^c \approx C_3^e \approx C_4^e \approx c. \tag{25}$$

In addition, we should consider the conditions of orbital overlap densities among the frontier orbitals (see Eqs (11) and (12)). Since $\phi_i(L)$ and $\phi_j(R)$ are the localized fragment MOs, $\phi_i(L)\phi_j(R) \approx 0$ ($i, j =$ HO, NHO, LU, and NLU). Accordingly,

$$|\psi_{\mathrm{LU}}|^2 \approx |\psi_{\mathrm{NLU}}|^2, \quad \psi_{\mathrm{HO}}\psi_{\mathrm{NLU}} \approx \psi_{\mathrm{NHO}}\psi_{\mathrm{LU}}, \quad |\psi_{\mathrm{HO}}|^2 \approx |\psi_{\mathrm{NHO}}|^2, \quad \psi_{\mathrm{HO}}\psi_{\mathrm{LU}} \approx \psi_{\mathrm{NHO}}\psi_{\mathrm{NLU}}, \tag{26}$$

$$\psi_{\mathrm{HO}}\psi_{\mathrm{NHO}} \neq \psi_{\mathrm{LU}}\psi_{\mathrm{NLU}}. \tag{27}$$

In general, these conditions can be satisfied in systems with pseudo-degenerate electronic states.

In order to elucidate the reason for the disappearance of the overlap densities shown in Fig. 7, we discuss the overlap densities between approximate excited wave functions.

(Case 1: Ψ_a and Ψ_e) This case corresponds to T_4–T_2. The overlap density between Ψ_a and Ψ_e is given by

$$\rho^{ae} = (C_1^a C_3^e + C_2^a C_4^e)\psi_{\mathrm{LU}}\psi_{\mathrm{NLU}} + (C_1^a C_4^e + C_2^a C_3^e)\psi_{\mathrm{HO}}\psi_{\mathrm{NHO}}. \tag{28}$$

From the condition for the CI coefficients, (Eq. 25),

$$C_1^a C_3^e + C_2^a C_4^e \approx 0, \quad C_1^a C_4^e + C_2^a C_3^e \approx 0. \tag{29}$$

Thus, the overlap density between Ψ_a and Ψ_e is cancelled out. Note that the disappearance of overlap density originates from the condition of the CI coefficients.

(Case 2: Ψ_a and Ψ_c) This case corresponds to T_4–T_1. The overlap density between Ψ_a and Ψ_c is given by

$$\rho^{ac} = C_1^a C_1^c(\rho_0 - |\psi_{\mathrm{HO}}|^2 + |\psi_{\mathrm{LU}}|^2) + C_2^a C_2^c(\rho_0 - |\psi_{\mathrm{NHO}}|^2 + |\psi_{\mathrm{NLU}}|^2). \tag{30}$$

From the condition for the CI coefficients,

$$\rho^{ac} \approx c^2(|\psi_{\mathrm{NHO}}|^2 - |\psi_{\mathrm{HO}}|^2 + |\psi_{\mathrm{LU}}|^2 - |\psi_{\mathrm{NLU}}|^2). \tag{31}$$

From the condition for the orbital densities, Eq. (26),

$$\rho^{ac} \approx 0. \tag{32}$$

Note that the disappearance of overlap density originates from the condition of the orbital densities of the frontier orbitals as well as that of the CI coefficients.

(Case 3: Ψ_b and Ψ_0) This case corresponds to S_2–S_0. The overlap density between Ψ_b and Ψ_0 is given by

$$\rho^{b0} \approx c(\psi_{\mathrm{HO}}\psi_{\mathrm{NLU}} - \psi_{\mathrm{NHO}}\psi_{\mathrm{LU}}). \tag{33}$$

According to Eq. (26), ρ^{b0} is cancelled out (see also Fig. S16 in the Supplemental Material). Note that the disappearance of overlap density originates from the condition of the orbital overlap densities of the frontier orbitals as well as that of the CI coefficients.

(Case 4: Ψ_b and Ψ_d) This case corresponds to S_2–S_1. According to Eq. (26), the overlap density between Ψ_b and Ψ_d is given by

$$\rho^{bd} \approx c(\psi_{\mathrm{NLU}}\psi_{\mathrm{LU}} - \psi_{\mathrm{NHO}}\psi_{\mathrm{HO}}) \neq 0. \tag{34}$$

Thus, ρ^{bd} is not cancelled out.

General cases are discussed in Section S11 of the Supplemental Material. The reduced overlap densities of Cases 1–3, which originate from the pseudo degeneracy, are responsible for the suppression of undesirable radiative and non-radiative transitions, $T_3 \rightarrow T_2$, $T_3 \rightarrow T_1$, and $S_2 \rightarrow S_0$, for the FvHT mechanism.

In conclusion, we proposed a *fluorescence via higher triplets* (*FvHT*) emitting mechanism for OLEDs based on a bisanthracene derivative, BD1. This mechanism is valid as long as all transitions from T_m ($m > 1$) to all lower T_n ($m > n \geq 1$) are suppressed. In BD1, we found that this condition is satisfied because of its pseudo-degenerate electronic structure. The undesirable radiative and non-radiative transitions can be suppressed by utilizing the pseudo-degeneracy. We also discussed general conditions for the suppression of radiative and non-radiative transitions in a pseudo-degenerate system. Recently, Hu *et al.* have reviewed the RISC from upper triplet levels to excited singlet[19]. Since some molecules are expected to have pseudo-degenerate electronic structures, the RISCs of such systems might be elucidated from the point of view of the present mechanism. The general conditions are applicable not only for transitions in a molecule, but also for exciton migrations in the solid phase. The design principle based on the FvHT mechanism allows the use of asymmetric molecules, differently from iST and SC-TADF based on the selection rules for a molecular symmetry group. Finally, we propose a superordinate concept, *fluorescence via RISC* (*FvRISC*) from T_1 or higher triplet states. This concept includes TADF, SC-TADF, iST, and FvHT. The concept of FvRISC enables us to overcome the singlet exciton formation ratio of 25% for electrical excitations and to realize highly efficient OLEDs with a wide variety of molecular structures and symmetries.

Methods

The optimized structure of BD1 in the ground state was obtained. The structure was confirmed to be the minimum energy structure using vibrational analysis. In order to discuss radiative and non-radiative transition processes from excited states, excited adiabatic (AD) states were obtained by carrying out geometry optimizations in the excited states. The normal modes were also obtained by vibrational analyses. The vibrational analyses were carried out for S_0 at the optimized structures for the excited states. These calculations were performed at the B3LYP/6-311 + G(d,p) and TD-B3LYP/6-311 + G(d,p) levels of theory for the ground and excited states, respectively. In the excited state calculations, ten singlet and ten triplet states were taken into consideration. Off-diagonal VCCs between triplet states T_m–T_n, as well as singlet states S_m–S_n, which govern the non-radiative transition rates, were calculated at the AD states. Furthermore, in order to analyze the results of the VCC calculations, VCD analyses were carried out for strong coupling modes. The electronic and vibrational states were calculated using Gaussian 09 Revision D.01[20], while the VCC calculations and VCD analyses were performed using our in-house codes.

References

1. Adachi, C. Third-generation organic electroluminescence materials. *Jpn. J. Appl. Phys.* **53**, 060101 (2014).
2. Endo, A. *et al*. Thermally activated delayed fluorescence from Sn^{4+}-porphyrin complexes and their application to organic light emitting diodes – a novel mechanism for electroluminescence. *Adv. Mater.* **21**, 4802–4806 (2009).
3. Tanaka, H., Shizu, K., Miyazaki, H. & Adachi, C. Efficient green thermally activated delayed fluorescence (TADF) from a phenoxazine-triphenyltriazine (PXZ-TRZ) derivative. *Chem. Commun.* **48**, 11392–11394 (2012).
4. Uoyama, H., Goushi, K., Shizu, K., Nomura, H. & Adachi, C. Highly efficient organic light-emitting diodes from delayed fluorescence. *Nature* **492**, 234–238 (2012).
5. Lee, S. Y., Yasuda, T., Nomura, H. & Adachi, C. High-efficiency organic light-emitting diodes utilizing thermally activated delayed fluorescence from triazine-based donor-acceptor hybrid molecules. *Appl. Phys. Lett.* **101**, 093306 (2012).
6. Nakagawa, T., Ku, S.-Y., Wong, K.-T. & Adachi, C. Electroluminescence based on thermally activated delayed fluorescence generated by a spirobifluorene donor-acceptor structure. *Chem. Commun.* **48**, 9580–9582 (2012).
7. Méhes, G., Nomura, H., Zhang, Q., Nakagawa, T. & Adachi, C. Enhanced electroluminescence efficiency in a spiro-acridine derivative through thermally activated delayed fluorescence. *Angew. Chem., Int. Ed.* **51**, 11311–11315 (2012).
8. Kaji, H. *et al*. Purely organic electroluminescent material realizing 100% conversion from electricity to light. *Nat. Commun.* **6**, 8476 (2015).
9. Sato, T. *et al*. Vibronic coupling density and related concepts. *J. Phys.: Conf. Ser.* **428**, 012010 1–19 (2013).
10. Uejima, M., Sato, T., Yokoyama, D., Tanaka, K. & Park, J.-W. Quantum yield in blue-emitting anthracene derivatives: vibronic coupling density and transition dipole moment density. *Phys. Chem. Chem. Phys.* **16**, 14244–14256 (2014).
11. Sato, T., Uejima, M., Tanaka, K., Kaji, H. & Adachi, C. A light-emitting mechanism for organic light-emitting diodes: molecular design for inverted singlet-triplet structure and symmetry-controlled thermally activated delayed fluorescence. *J. Mater. Chem. C* **3**, 870–878 (2015).
12. Yao, L. *et al*. Highly efficient near-infrared organic light-emitting diode based on a butterfly-shaped donor-acceptor chromophore with strong solid-state fluorescence and a large proportion of radiative excitons. *Angew. Chem., Int. Ed.* **126**, 2151–2155 (2014).
13. Sato, T. Fluorescence via reverse intersystem crossing from higher triplet states. *J. Comput. Chem., Jpn* **14**, 189–192 (2015).
14. Longuet-Higgins, H. C. The Electronic States of Composite Systems. *Proc. R. Soc. London, Ser. A* **235**, 537–543 (1956).
15. Hayashi, M. *et al*. Ab initio calculations of radiationless transitions between excited and ground singlet electronic states of ethylene. *J. Chem. Phys.* **108**, 2044–2055 (1998).
16. Niu, Y. *et al*. Theory of Excited State Decays and Optical Spectra: Application to Polyatomic Molecules. *J. Phys. Chem. A* **114**, 7817–7831 (2010).
17. Fischer, G. *Vibronic Coupling: The Interaction Between the Electronic and Nuclear Motions*. Academic Press, London (1984).
18. Hu, J.-Y. *et al*. Bisanthracene-based donor-acceptor-type light-emitting dopants: Highly efficient deep-blue emission in organic light-emitting devices. *Adv. Funct. Mater.* **24**, 2064–2071 (2014).
19. Hu, D. *et al*. Reverse intersystem crossing from upper triplet levels to excited singlet: a 'hot excition' path for organic light-emitting diodes. *Phil. Trans. R. Soc. A* **373**, 20140318 1–16 (2015).
20. Frisch, M. J. *et al*. Gaussian 09 Revision D.01 http://gaussian.com/ (Gaussian Inc., Wallingford CT 2009.)

Acknowledgements

We thank Prof. Hirofumi Sato. Numerical calculations were partly performed at the Supercomputer Laboratory of Kyoto University and at the Research Center for Computational Science, Okazaki, Japan. This study was also supported by JSPS KAKENHI Grant Number JP15K05607 in Scientific Research (C) and JSPS KAKENHI Grant Number JP17H05259 in Scientific Research on Innovative Areas "Photosynergetics".

Author Contributions

T.S. and Y.-J. Pu conceived and supervised the work. R.H. calculated vibronic couplings between excited and ground states with TD-DFT. N.H. and T.S. analyzed the origin of RISC from higher triplet states to singlet states and derived a general condition for the RISC. All authors participated to the discussion of the results and the writing of the manuscript.

Additional Information

Supplementary information accompanies this paper at doi:10.1038/s41598-017-05007-7

Competing Interests: The authors declare that they have no competing interests.

Publisher's note: Springer Nature remains neutral with regard to jurisdictional claims in published maps and institutional affiliations.